

**Figure 2.** Electronic absorption (middle) and MCD (top) spectra of  $H_4Pc_2$  in  $CHCl_3$ . The absorption spectrum of octabutoxylated  $H_2Pc$  in  $CHCl_3$  is also shown for comparison (bottom).

U-3410 spectrophotometer at room temperature. Magnetic circular dichroism (MCD) measurements were made at room temperature with a JASCO J-725 spectropolarimeter equipped with a JASCO electromagnet that produced magnetic fields of up to 1.09 T with parallel and then antiparallel fields. Its magnitude was expressed in terms of molar ellipticity per tesla,  $[\theta]_M/\text{deg mol}^{-1} \text{ dm}^3 \text{ cm}^{-1} \text{ T}^{-1}$ .

Deconvolution of the pairs of associated absorption and MCD spectral data that had been separated into the Soret (260–550 nm) and Q (500–1000 nm) regions was carried out by using the program SIMPFIT<sup>11</sup> on a DELL OptiPlex GXi computer.

**Theoretical Calculations.** The results of the Pariser–Parr–Pople (PPP) LCAO-CI calculations were quoted from a previous publication.<sup>6</sup> However, we will add further information that was not published in ref 6.

## Results and Discussion

**Spectroscopy.** Figure 2 shows the electronic absorption (middle) and MCD (top) spectra of  $H_4Pc_2$  in  $CHCl_3$ . The absorption spectrum of octabutoxylated  $H_2Pc$  in  $CHCl_3$  (bottom) is also shown for comparison. Compared with the mononuclear  $H_2Pc$ , the Q band of  $H_4Pc_2$  is considerably red-shifted and broadened (ca. 550–900 nm), whereas the positions of their Soret bands are very close (near 350 nm) to each other. In the Q-band region, at least two intense bands are included at ca. 840 and 750 nm. The 840 nm band is not symmetrical and suggests an involvement of more than one component. A broad band with intermediate intensity at ca. 400–500 nm is commonly seen for Pcs with peripheral alkoxy or alkylthio groups and has been assigned to an  $n \rightarrow \pi^*$  transition involving ether oxygen or thioether sulfur lone pairs.<sup>12</sup> Its intensity increases with increasing number of these groups. In the MCD spectrum

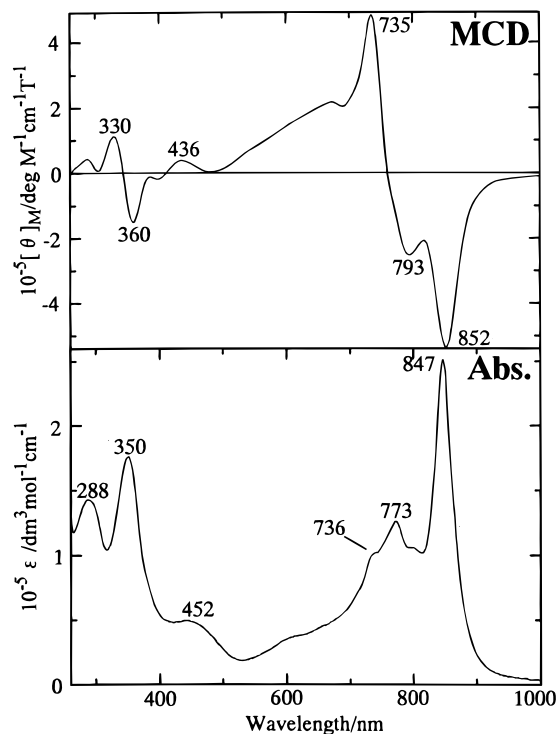


**Figure 3.** Absorption (bottom) and MCD (top) spectra of  $Cu_2Pc_2$  in  $CHCl_3$ .

**Table 1.** Absorption and MCD Data in  $CHCl_3$

compound	absorption <sup>a</sup>			MCD <sup>b</sup>	
	$\lambda/\text{nm}$	$\epsilon/\text{dm}^3 \text{ mol}^{-1} \text{ cm}^{-1}$	$\lambda/\text{nm}$	$[\theta]_M/\text{deg dm}^3 \text{ mol}^{-1} \text{ cm}^{-1} \text{ T}^{-1}$	$[\theta]_M/\text{deg dm}^3 \text{ mol}^{-1} \text{ cm}^{-1} \text{ T}^{-1}$
$H_4Pc_2$	301(1.01)	354(1.76)	288(0.51)	382(1.37)	361(-2.46)
	447(0.60)	664(0.43)	435(0.30)	482(-0.38)	670(2.64)
	748(1.18)	838(2.38)	721(4.78)	738(6.62)	770(-1.64)
$Cu_2Pc_2$			796(-2.24)	840(-5.75)	
	288(1.42)	350(1.76)	330(0.78)	360(-1.02)	436(0.31)
	452(0.48)	736(1.00)	735(2.70)	793(-2.88)	852(-4.13)
			773(1.26)	847(2.57)	

<sup>a</sup>  $\lambda/\text{nm}$  ( $10^{-5}\epsilon/\text{M}^{-1} \text{ cm}^{-1}$ ). <sup>b</sup>  $\lambda/\text{nm}$  ( $10^{-5}[\theta]_M/\text{deg dm}^3 \text{ mol}^{-1} \text{ cm}^{-1} \text{ T}^{-1}$ ).

of  $H_4Pc_2$ , a large trough and a peak are observed at 840 and 738 nm, respectively, suggesting that these are mutually interacting transitions. A noteworthy point is that the 738 nm peak position is shifted to the blue by 10 nm from the 748 nm peak seen in the absorption spectrum, although the 840 nm trough is shifted by only 2 nm from the corresponding absorption peak. MCD curves that change sign from minus to plus on going from longer to shorter wavelengths were recorded corresponding to the absorption peaks at 447, 354, and 301 nm.

Deprotonation of  $H_4Pc_2$  was attempted by adding aliquots of tetra-*n*-butylammonium hydroxide (ca. 20% in methanol) dropwise to a  $CHCl_3$  solution of  $H_4Pc_2$  while monitoring the absorption spectra, since the PPP method considers only the  $\pi$  framework and the deprotonated form matched up for comparison. However, reasonable spectra were not obtained during the deprotonation because of instability of the solution.

Figure 3 shows the absorption and MCD spectra of  $Cu_2Pc_2$  in  $CHCl_3$ , with data for this and for  $H_4Pc_2$  listed in Table 1. The Q bands still split into two peaks at ca. 850 and 770 nm because the molecule has  $D_{2h}$  symmetry. Although the shapes of the spectra are similar to that of  $H_4Pc_2$ , all bands become slightly sharper. In addition, the longest wavelength Q<sub>00</sub> band became more symmetrical compared with that of  $H_4Pc_2$ . If we take the position of the pyrrole protons into account,  $H_4Pc_2$  is considered to exist as a mixture of several isomers. Accordingly,

(11) Browett, W. R.; Stillman, M. J. *J. Comput. Chem.* **1987**, *11*, 73.

(12) (a) Kobayashi, N.; Lever, A. B. P. *J. Am. Chem. Soc.* **1987**, *109*, 7433.

(b) Guo, L.; Ellis, D. E.; Hoffman, B. M.; Ishikawa, Y. *Inorg. Chem.* **1996**, *35*, 5304.

**Table 2.** Band Fitting Parameters for Cu<sub>2</sub>Pc<sub>2</sub> in CHCl<sub>3</sub><sup>a</sup>

band no.	$\nu/\text{cm}^{-1}$	$\lambda/\text{nm}$	$\epsilon_{\text{max}}$	MCD intens	$\Delta\nu/\text{cm}^{-1}$	$D_0$	$\langle\epsilon\rangle_0$	$\langle\epsilon_M\rangle_0$	$B_0$	$B_0/D_0$	$f$
1	39854	251	230608	-121561	1698	32	10462	-5515	-36.2	-1.13	1.80
2	38140	262	91586	7412	2198	17.2	5619	455	2.98	0.17	0.93
3	36481	274	62151	5141	2133	11.8	3868	320	2.1	0.18	0.61
4	34591	289	127160	45391	3153	37.8	12339	4405	28.9	0.76	1.84
5	32711	306	63118	-24447	2234	14.1	4589	-1777	-11.7	-0.83	0.65
6	31264	320	45968	52482	1989	9.53	3113	3554	28.3	2.44	0.42
7	29499	339	117153	111808	2625	34	11097	10591	69.4	2.04	1.41
8	28018	357	113329	-190922	2131	28.1	9174	-15456	-101	-3.59	1.11
9	26067	384	61689	4001	2244	17.3	5653	367	2.4	0.14	0.64
10	24626	406	17513	-26060	1519	3.52	1150	-1711	-11.2	-3.18	0.12
11	23334	429	41695	36087	2004	11.7	3811	3299	21.6	1.85	0.38
12	22102	452	19849	16666	1489	4.36	1423	1195	7.83	1.8	0.14
13	20885	479	35131	-2489	2119	11.6	3795	-269	-1.76	-0.15	0.34
14	19100	524	12988	33167	1669	3.7	1208	3085	20.2	5.46	0.10
15	18031	555	15268	69936	1113	3.07	1003	4595	30.1	9.8	0.0781
16	19971	501	23171	9673	1091	4.12	1347	562	3.89	0.94	0.12
17	19162	522	8622	16225	1060	1.55	507.8	956	6.27	4.05	0.042
18	18239	548	18065	68852	1319	4.26	1391	5302	34.8	8.17	0.11
19	16969	589	29520	115894	1269	7.19	2350	9225	60.5	8.41	0.17
20	16021	624	30472	137237	952	5.9	1927	8677	56.9	9.64	0.13
21	15399	649	26189	126958	650	3.6	1176	5703	37.4	10.4	0.0783
22	14737	679	46968	197529	845	8.78	2867	12058	79.1	9.01	0.18
23	14099	709	48523	150143	653	7.33	2393	7405	48.6	6.63	0.15
24	13561	737	83628	452309	631	12.7	4145	22417	147	11.6	0.24
25	12948	772	116512	-185337	661	19.4	6334	-10075	-66.1	-3.41	0.35
26	12361	809	87518	-203594	535	12.3	4033	-9383	-61.5	-5	0.22
27	11822	846	207501	-383488	444	25.4	8298	-15334	-101	-3.98	0.42
28	11491	870	50868	-222677	722	10.4	3402	-14893	-97.7	-9.39	0.17
29	10528	950	6754	-16134	737	1.54	503.3	-1202	-7.88	-5.12	0.0229

<sup>a</sup>  $D_0$  (dipole strength) =  $\langle\epsilon\rangle_0/326.6$ .  $\langle\epsilon\rangle_0$  is the zeroth moment of the MCD.  $B_0 = \langle\epsilon_M\rangle_0/152.5$ .  $f$  is the oscillator strength.

the spectrum of Cu<sub>2</sub>Pc<sub>2</sub> is thought to become sharper because of the decrease in the number of isomers. Again, an intense positive MCD band at 735 nm is markedly shifted from the second intense absorption band (773 nm) in the Q-band region.

**Band Deconvolution Analyses.** We decided to choose the copper complex, Cu<sub>2</sub>Pc<sub>2</sub>, for band deconvolution analyses because its symmetry is the same as that of the  $\pi$  framework. Band deconvolution, which isolates the required bands from spectra by fitting each band with a Gaussian line shape, has been rigorously developed by Stillman et al. and is virtually the only way of accessing the transitions responsible for bands that overlap to any extent. As has been reported previously,<sup>13</sup> linking the absorption and MCD spectra remarkably enhanced the reliability of band deconvolution calculations. In other words, band centers and bandwidths have been kept identical for the associated bands in both spectra to reduce the ambiguity of the results. By this technique, many bands have been definitely assigned, and even unknown transitions that were not predicted by calculations because of the intensity being too low were found and assigned. Although Stillman et al. reported that measurements of absorption and MCD spectra at cryogenic temperature were better for detailed discussions,<sup>13j</sup> we were able to obtain satisfactory spectra at ambient temperature. Parts A and B of Figure 4 show the results of band analyses for the Soret and the Q-band regions, respectively. All derived param-

eters are summarized in Table 2. Deconvolution of the spectra required 29 overlapping bands to fill the envelope in the entire region. Plotted below the absorption spectra are the differences between the experimental and deconvoluted absorption spectra. The randomness of the noise suggests little systematic error. Since the molecule has  $D_{2h}$  symmetry, the doubly degenerate bands of monomeric MPc with  $D_{4h}$  symmetry split into two bands. Because the resulting pairs of orbitals still lie reasonably close in energy, transitions into these orbitals will mix under the influence of the applied magnetic field to give rise to pairs of intense oppositely signed  $B$  terms in the MCD spectrum.<sup>14</sup> Thus, we judged that bands 4 and 5 originate from the N band, while bands 7 and 8 are split components of the B (Soret) band. In the Q-band region, bands 24 and 27 are safely assigned to the split  $Q_{00}$  transitions ( $Q_{y00}$  and  $Q_{x00}$ , respectively), since the corresponding  $B$  terms show opposite signs. Although the splittings in the N and B bands appear much smaller than that in the Q band in these figures, the calculated splittings are roughly similar (1880, 1481, and 1739  $\text{cm}^{-1}$  in this order, Table 2). In the Q-band region, bands 25 and 26 are vibronic progressions of band 27 ( $Q_{x00}$ ) while bands 20–23 would be those of band 24 ( $Q_{y00}$ ). Interestingly, the relative strength of and energy separation among bands 25–27 are very close to those seen in normal monomeric MPcs.<sup>15,16</sup> For example, the energy separation between the  $Q_{00}$  and  $Q_{01}$  bands in normal MPc with  $D_{4h}$  symmetry is considered to be ca. 1.1  $\text{kcm}^{-1}$ , while in Figure 4B, the energy difference between bands 27 and 25 is 1126  $\text{cm}^{-1}$ . Normal MPcs often show a small absorption peak

(13) (a) Nyokong, T.; Gasyana, Z.; Stillman, M. J. *Inorg. Chem.* **1987**, *26*, 1087. (b) Browett, W. R.; Gasyana, Z.; Stillman, M. J. *J. Am. Chem. Soc.* **1988**, *110*, 3633. (c) Ough, E. A.; Nyokong, T.; Creber, K. A. M.; Stillman, M. J. *Inorg. Chem.* **1988**, *27*, 2724. (d) Gasyana, T.; Kobayashi, N.; Stillman, M. J. *J. Chem. Soc., Dalton Trans.* **1989**, 2397. (e) Gasyana, Z.; Stillman, M. J. *Inorg. Chem.* **1990**, *29*, 5101. (f) Ough, E. A.; Gasyana, Z.; Stillman, M. J. *Inorg. Chem.* **1991**, *30*, 2301. (g) Mack, J.; Stillman, M. J. *Inorg. Chem.* **1992**, *31*, 1717. (h) Ough, E. A.; Stillman, M. J. *Inorg. Chem.* **1994**, *33*, 573. (i) Mack, J.; Stillman, M. J. *J. Am. Chem. Soc.* **1994**, *116*, 1292. (j) Mack, J.; Stillman, M. J. *J. Phys. Chem.* **1995**, *99*, 7935. (k) Mack, J.; Stillman, M. J. *Inorg. Chem.* **1997**, *36*, 413. (l) Mack, J.; Kobayashi, N.; Leznoff, C. C.; Stillman, M. J. *Inorg. Chem.* **1997**, *36*, 5624. (m) Ough, E. A.; Creber, K. A. M.; Stillman, M. J. *Inorg. Chim. Acta* **1996**, *246*, 361.

(14) Two interacting  $B$  terms produce MCD peaks of opposite signs. Tajiri, A.; Winkler, J. Z. *Naturforsch.* **1983**, *38a*, 1263. Kaito, A.; Nozawa, T.; Yamamoto, T.; Hatano, M.; Orii, Y. *Chem. Phys. Lett.* **1977**, *52*, 154.

(15) Stillman, M. J.; Nyokong, T. In *Phthalocyanines—Properties and Applications*; Leznoff, C. C., Lever, A. B. P., Eds.; VCH: New York, 1989; Vol. 1, Chapter 3.

(16) Kobayashi, N. In *Phthalocyanines—Properties and Applications*; Leznoff, C. C., Lever, A. B. P., Eds.; VCH: New York, 1990; Vol. 2, Chapter 3.



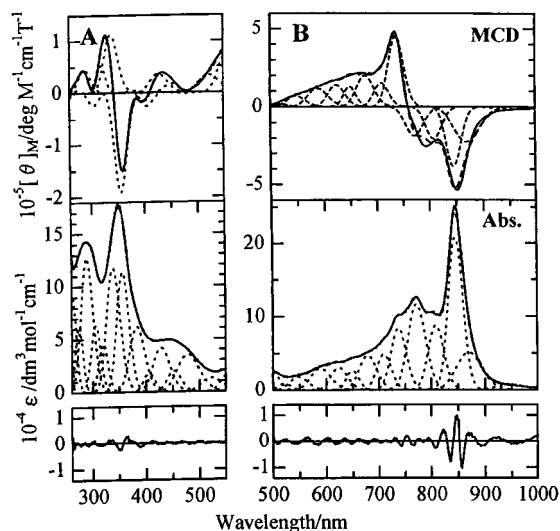


**Figure 4.** Deconvolution analysis of the (A) 260–550 and (B) 500–1000 nm spectral regions of  $\text{Cu}_2\text{Pc}_2$ : (—) experimental data; (---) fitted data; (···) individual bands. The parameters used are summarized in Table 2.

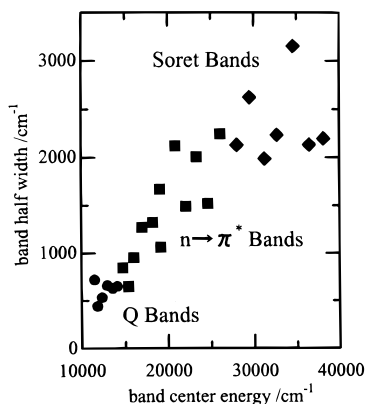


**Figure 5.** Scatter plot of the bandwidths used in Figure 4 as a function of the energy of the band center. The symbols indicate bandwidths taken from the following regions of the spectrum: (circles) Q band near 800 nm; (squares)  $n-\pi^*$  bands near 450 nm; (diamonds) Soret band near 350 nm. The boundary region between the Q band and  $n-\pi^*$  band is not clear.

midway between the  $Q_{00}$  and  $Q_{01}$  bands. The assignment of this band has not been confirmed, and in Figure 4B, band 26 corresponds to this band. The energy separation from band 27 ( $Q_{x00}$ ) is  $539\text{ cm}^{-1}$ , which is roughly comparable to that of  $\text{ZnPc}$  ( $660\text{ cm}^{-1}$ ).<sup>17</sup> We found these phenomena by chance, after band deconvolution analysis. However, they appear to be a consequence of quite natural events because our dimers consist of two MPc units and their frontier orbitals are expressed as linear combinations of MOs of constituting monomers.<sup>6</sup> The relatively large discrepancy of the  $Q_{y00}$  MCD peak and the second most intense Q absorption band positions is thus attributed to the superimposition of the  $Q_{x01}$  and  $Q_{y00}$  absorption bands.

In the  $n-\pi^*$  transition region between 400 and 500 nm, two components with intermediate intensity (bands 11 and 13) were required together with small bands 10 and 12. Bands 9 and 10 may be the split components of what we call the B1 band,<sup>13</sup> judging from their location.

Figure 5 compares the bandwidths calculated in the fit with the band maxima energy; an almost linear dependence is observed, as Hochstrasser and Marzacco described on the

manifold of singlet  $\pi-\pi^*$  and  $n-\pi^*$  excited states of small aromatic and heteroaromatic molecules.<sup>18</sup> The bandwidths of transitions to the higher states is broadened because of energy uncertainty deriving from their natural radiative lifetimes. Although this kind of wide range of data is reported for the reduced form of a phthalocyanine,<sup>13i</sup> Figure 5 represents the first report of the effect on a neutral species in any porphyrin or phthalocyanine.

**Comparison with Molecular Orbital Calculations.** Molecular orbitals, transition energies, and oscillator strengths for deprotonated planar bisphthalocyanine, calculated using the PPP method, were reported previously.<sup>6</sup> However, they were not necessarily detailed enough for the present study. Accordingly, the details of the results for deprotonated  $\text{H}_4\text{Pc}_2$  are summarized in Table 3. As seen in this table, the split  $Q_{00}$  bands are estimated at 847 and 682 nm with an intensity ratio of 1.66 ( $=2.21:1.33$ ). These are very close to the results of the band deconvolution analysis (Table 2). Indeed, the  $Q_{x00}$  and  $Q_{y00}$  bands are found at 846 and 737 nm, respectively, and their intensity ratio is 1.75 ( $=0.42:0.24$ ).<sup>19</sup> The split B (Soret) bands were calculated at 342 and 333 nm for experimental 357 and 339 nm, and the theoretical intensity ratio of 0.80 ( $=3.34:4.18$ ) is almost the same as the experimentally obtained value of 0.79 ( $=1.11:1.41$ ).

Two additional bands are calculated to lie at the longer wavelength side of the B (Soret) band. These are, judging from the configuration, mainly  $\text{HOMO} - 1 \rightarrow \text{LUMO} + 2$  (479 nm) and  $\text{HOMO} \rightarrow \text{LUMO} + 3$  (393 nm) transitions. We cannot determine which bands in Table 2 correspond to these transitions. However, since the energy and intensity of both the Q and B bands are being reproduced very well, these bands are deduced to lie at around 480–490 and 390–400 nm, respectively. Namely, these bands overlap with the  $n-\pi^*$  transitions of ether oxygen. However, of the absorptions in the region of ca. 400–500 nm, the contribution of these transitions appears small, since the calculated intensity is about 8.5% of that of the Q band and 4% of the B band. Although not for oxygen, Hoffman et al. reported the results of MO calculations of thioether-substituted tetraazaporphyrins with several types of symmetry and commented on the  $n-\pi^*$  transitions of sulfur.<sup>12b</sup> According to their results, these bands appear to the red of the Soret band and two transitions were calculated in proximity. That to longer wavelength is a transition between two MOs that have large coefficients of  $C\alpha$  and  $C\beta$  (2p) and small coefficients of S (3p), while the other transition to shorter wavelength is a charge-transfer transition from an S 3p centered orbital to the tetraazaporphyrin-centered orbital, which contains a large contribution of N 2p orbital. They commented also that in the case of ether oxygen, electrons in O 2p orbitals behave similarly to those in S 3p orbitals.

In the case of normal MPcs, the N band that arises from the very complicated mixture of atomic orbitals is observed to the higher energy side of the B band, and their energy difference is ca.  $5-6\text{ kcm}^{-1}$  both experimentally<sup>13a,m,16</sup> and theoretically.<sup>20</sup> Accordingly, an absorption peak next to the B band to higher energy is generally assigned to this band. In the case of  $\text{Cu}_2\text{Pc}_2$ , the band at 288 nm (Figure 3) whose energy difference from the B band (350 nm) is ca.  $6.15\text{ kcm}^{-1}$  appears to correspond to this band. In the absorption spectrum, this peak appears to be a single peak, since even the B band, which lies

(18) Hochstrasser, R. M.; Marzacco, C. *J. Chem. Phys.* **1968**, *49*, 971.

(19) In the Q-band spectra of normal MPc, both the  $Q_{00}$  and  $Q_{01}$  bands have some intensity while the  $Q_{02}$  band is very weak.<sup>15</sup> Accordingly, if we count bands 25–27 as the  $Q_x$  and bands 22–24 as the  $Q_y$  band, their intensity ratio becomes 1.74 ( $=0.99/0.57$ ).

(17) Kobayashi, N. Unpublished results.

**Table 3.** Calculated Transition Energies, Oscillator Strength ( $f$ ), and Configurations for  $\text{Pc}_2^{4-}$  <sup>a</sup>

energy/eV	energy/nm	$f$	configuration <sup>b</sup>		
1.465	847	2.21	39 → 40(88%)		
1.817	682	1.33	39 → 41(71%)	38 → 42(13%)	
2.588	479	0.16	38 → 42(77%)	39 → 41(18%)	
3.159	393	0.14	39 → 44(65%)	38 → 45(16%)	38 → 43(14%)
3.624	342	3.34	37 → 41(42%)	36 → 42(25%)	38 → 43(14%)
3.721	333	4.18	37 → 40(49%)	36 → 43(13%)	24 → 40(11%)
3.939	315	0.30	30 → 40(37%)	39 → 48(17%)	24 → 40(11%)
4.071	305	0.19	39 → 49(30%)	25 → 42(11%)	30 → 41(10%)
			24 → 41(10%)		
4.081	304	0.33	26 → 41(17%)	28 → 40(15%)	27 → 42(13%)
			24 → 40(11%)		
4.113	301	0.12	26 → 41(26%)	27 → 42(23%)	39 → 48(19%)
4.186	296	0.50	39 → 49(36%)	31 → 40(13%)	
4.337	286	0.11	31 → 40(19%)	38 → 45(16%)	37 → 41(13%)
			24 → 41(12%)		
4.493	276	0.30	31 → 41(25%)	24 → 40(21%)	30 → 40(13%)
4.666	266	0.48	36 → 43(61%)		

<sup>a</sup> Excited states with less than 4.7 eV and  $f$  greater than 0.10 are shown. <sup>b</sup> Orbital number 39 is the HOMO of  $\text{Pc}_2^{4-}$ .

at longer wavelengths, looks like a single peak.<sup>20</sup> However, at least theoretically, this band is split into  $D_{2h}$  type species such as we have here. Our band deconvolution showed at least three components (bands 3–5, Table 2) below this peak (Figure 4A). The band in the center (band 4) is particularly intense in comparison to the other bands. If we compare the band deconvolution results with those of the MO calculations in Table 3, it is seen that a series of weak bands are estimated to lie between 296 and 305 nm. Since these bands are so close in energy, they may appear as a single component in Figure 4A. These components therefore may all be coalesced together in band 4. The calculated intensity in this region appears to be too weak compared with experimental results. That is, adding the calculated oscillator strengths of the components that lie between 250 nm and shorter than the B band (2.33) gives a value about 32% that of the B band (7.52), while in experiments (Figure 4A) the strengths look almost comparable.

As shown in Table 3, the Q bands and Soret bands originate in transitions from HOMO to LUMO, LUMO + 1 and HOMO – 1 to LUMO + 2, LUMO + 3, respectively. Of these, we can find the combinations of the states that have angular momenta as follows. Since the symmetry of  $\text{Cu}_2\text{Pc}_2$  is  $D_{2h}$ , direct products should have an irreducible representation of  $B_{1g}$  in order to have nonzero matrix element values. Thus,  $\Gamma_{\text{state}1} \times \Gamma_{\text{state}2} = \Gamma_{B_{1g}}$ , and  $\langle \text{state}1 | l_z | \text{state}2 \rangle \neq 0$ , where  $\Gamma_x$  means an irreducible representation of state  $x$  and  $l_z$  is an orbital angular momentum operator. Concretely, it turns out that only two combinations, i.e., LUMO ( $a_u$ ) and LUMO + 1 ( $b_{1u}$ ) (the Q band), and LUMO + 2 ( $b_{2g}$ ) and LUMO + 3 ( $b_{3g}$ ) (the Soret band), are possible. That is, it is reasonably expected from the molecular orbital study that the B (Soret) and Q bands each show two MCD signals.

## Conclusion

The electronic absorption and MCD spectra of planar binuclear phthalocyanines have been analyzed using a band deconvolution technique and the results compared with those of molecular orbital calculations. As visually compared in Figure 6, the results of the band deconvolution analysis are in fairly good agreement with those of the PPP calculations. Thus, this

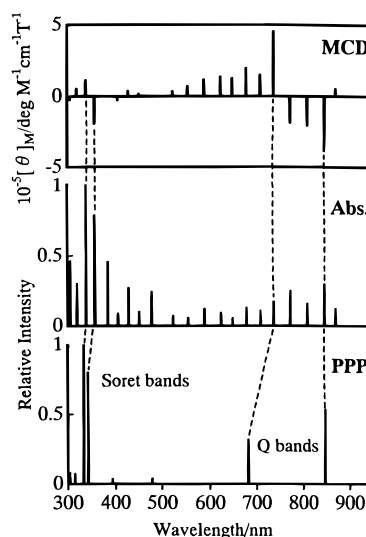


**Figure 6.** Comparison between the results of the band analysis (top and middle) with those of the PPP MO calculations (bottom). The vertical axes of two lower graphs represent relative intensity of oscillator strength.

study has demonstrated and reconfirmed that simultaneous band deconvolution of both the electronic absorption and MCD spectral envelopes is a powerful and useful technique for elucidating the electronic structure of large molecules such as phthalocyanines. We also stress the validity of MO calculations of large molecules within the framework of the PPP approximations that were first reported in the middle of this century.<sup>21</sup> Although the PPP method was applied to porphyrin systems almost 37 years ago,<sup>20</sup> no subsequent theoretical calculations have been reported that account for the band energies, dipole strengths, and angular momentum properties of the major transitions of MPcs in a more satisfactory manner.<sup>22,23</sup> The PPP

(20) Even if the splitting in the N band is approximately similar to that in the B band, the splitting in the absorption peak would not be perceived, since the splitting in the B band, which lies at longer wavelength, is difficult to detect.

- (21) Pariser, P.; Parr, R. G. *J. Chem. Phys.* **1953**, *21*, 466, 767. Pople, J. A. *Trans. Faraday Soc.* **1953**, *49*, 1375.  
 (22) (a) Hendricksson, A.; Roos, B.; Sundbom, M. *Theor. Chim. Acta* **1972**, *27*, 303. (b) Orti, E.; Bredas, J. L.; Clarisse, C. *J. Chem. Phys.* **1990**, *92*, 1228. (c) Ishikawa, N.; Ohno, O.; Kaizu, Y.; Kobayashi, H. *J. Phys. Chem.* **1992**, *96*, 8832. (d) Ishikawa, N.; Ohno, O.; Kaizu, Y. *J. Phys. Chem.* **1993**, *97*, 1004.  
 (23) Schaffer, A. M.; Gouterman, M.; Davidson, E. R. *Theor. Chim. Acta* **1973**, *30*, 9. Dedieu, A.; Rohmer, M.-M.; Veillard, A. *Adv. Quantum Chem.* **1982**, *16*, 43. Liang, X. L.; Flores, S.; Ellis, D. E.; Hoffman, B. M.; Musselman, R. L. *J. Chem. Phys.* **1991**, *95*, 403. Rosa, A.; Baerends, E. J. *Inorg. Chem.* **1992**, *31*, 4717; **1994**, *33*, 584.

method has been proven to be very useful in analyzing the spectra of low-symmetrical monomeric Pc derivatives.<sup>24</sup> This paper further demonstrates that it is useful even for molecules of the size of a Pc dimer.

---

(24) Kobayashi, N.; Konami, H. In *Phthalocyanines—Properties and Applications*; Leznoff, C. C., Lever, A. B. P., Eds.; VCH: New York, 1996; Chapter 9.

**Acknowledgment.** This research was supported partially by a Grant-in-Aid for Scientific Research (B) No. 11440192 and that on Priority Area “Creation of Delocalized Electron Systems” No. 12020206, from the Ministry of Education, Science, Sports, and Culture, Japan, and the Scandinavia–Japan Sasakawa Foundation.

IC991496S